GEOPERSIA

Accepted Manuscript

Kinematics of the Mezaijaan salt glacier based on InSAR data in the interior Fars of the Zagros Fold and Thrust Belt, Iran

Arash Jamshidy, Saeed Madanipour, Zahra Mousavi

DOI: 10.22059/GEOPE.2025.389864.648803

Receive Date: 03 February 2025
Revise Date: 26 April 2025
Accept Date: 03 May 2025

Kinematics of the Mezaijaan salt glacier based on InSAR data in the interior Fars of the Zagros Fold and Thrust Belt, Iran

Arash Jamshidy [1]. Saeed Madanipour [1, *], Zahra Mousavi [2]

[1] Department of Geology, Tarbiat Modares University, Tehran, Iran
[2] Department of Earth Sciences, Institute for Advanced Studies in Basic Sciences (IASBS), Zanjan, Iran

Received: 03 February 2025, Revised: 26 April 2025, Accepted: 03 May 2025

Abstract
The study of subaerial salt diapirs kinematics plays an important role in exploiting them as a host of resources, the objective of engineering operations or preventing the risks associated with them, The Zagros Fold and Thrust Belt (ZFTB) is a well-known host of salt diapirs across the world provided natural examples for exploring the interaction between internal forces driving salt extrusion, surface processes and climate which vanish them. The Mazaayjaan (MZJ) subaerial salt dome as one of the active subaerial salt dome which located in a near flat region, with an arid climate and sparse vegetation was selected as a unique candidate to answer the question how interaction of internal and surficial process shape a salt glacier; in this study the Interferometric Synthetic Aperture Radar is used as a main tool to constrain surface displacement, therefor the Sentinel 1A SLC images in ascending and descending orbits were processed by the StaMPS algorithm to extract surface displacement time-series, then jointly analyzed with geomorphic properties and weather records to clarify the relation between them, The results show a maximum of 15 mm/year in the vertical and 30 mm/year in the horizontal for MZJ surface deformation; the observed uplift rates in conjunction with other lines of evidence suggest that active shortening across the belt plays the main role in salt extrusion while sedimentation has a negligible role, at the surface, the gravity spreading which facilitated by the weakening effects of meteoric waters is the main vanishing factor, the entire body of MZJ shows a strong seasonality in which its displacement accelerates or decelerates by wet and dry periods while temperature fluctuation has no noticeable effect.

Keywords: Salt Glacier, Zagros Fold Thrust Belt, InSAR, Time Series, Gravity Spreading, Precipitation.

Introduction

Salt glaciers as surface manifestations of salt structures are abundant features of the Zagros Fold-Thrust belt in the Arabia-Eurasia collision zone. They distribute in different structural zones of the Zagros orogen from the High Zagros in the north to the foredeep part of the foreland basin as islands along the Persian Gulf coast in the south (Kent, 1970; Ala, 1974). They represent different morphological characteristics that are solely dependent on their kinematic path, salt intrinsic properties, and subaerial properties that salt emerged on it (Talbot & Pahjola, 2009). Previous studies have focused on salt structures because of their inherent characteristics and abundance of them in many parts of the sedimentary cover in the orogenic belts (Hudec & Jackson, 2007). Salt rocks are considered as a mobile material in the sedimentary cover because of low specific gravity and shear strength that decouples deformation between different units or upward motion through overlying stratas (Dahlstrom ,1990; Homza & Wallace,1995). All these properties make the salt related structures as important hydrocarbon traps then, a detailed

* Corresponding author e-mail: Madanipour.saeed@modares.ac.ir

study of them is essential for successful hydrocarbon exploration and production salt rock and related structures represent very low permeability which makes them ideal for fuels, and nuclear waste storage if their activity is very low for a long time (Allen, 1972; Jackson & Talbot, 1986). Salt bodies behave like fluids in geological time scale when exerted to differential loading result from movement in extensional and contractional tectonic settings, the gravitational load of internal body force of salt rock or weight of upper units and thermal loads (Hudec and Jackson, 2007). Salt bodies when reached to the surface in contact with surficial water dissolve and contaminate water resources (Zarei et al., 2012) or gravitationally spread under their weight and make Namakiers (salt glaciers) (Ajayebi & Amrikazemi, 2023).

The surface displacement of salt bodies are result of the interaction between internal forces which mainly includes tectonics and sedimentation that control the uplift or feeding rate of salt bodies, climatic variables, and surficial conditions (Talbot & Rogers, 1980; Hudec & Jackson, 2007; Aftabi et al., 2010; Kravitz, 2017). The flow rate of salt rock varies according to their tectonic settings and movement mechanism. The flow rate of the salt diapirs in Zagros has been reported in different scales in the previously published data. Player, (1969) suggested 0.3 - 2 mm/year for diapiric rise in the Zagros mountainous belt. Dating of coral reefs around the salt domes in Yemen suggested ~0.3 mm/year for diapiric rise but when the salt breaks the surface, the dome rises at a rate of 4.6 mm/year (Davison et al., 1996). The same method has been used for coral reefs around salt cored islands of Hormuz and Qeshm in the Persian Gulf showing the rate of 1-6 mm/year (Bruthan et al., 2008). Accoridng to the land surveying of Jahani (Talbot et al., 2000) and Konarsiah (Zarei et al., 2012), salt glaciers indicate 2-5 m/year for vertical and horizontal flow rates which varied seasonally.

Unlike the above-mentioned methods that are based on measurement at special points, Interferometric Synthetic Aperture Radar (InSAR) has large spatial coverage, high accuracy, and acceptable temporal and spatial resolution so that has been widely used in recent years to study land surface changes (Massonnet et al. 1993; Bürgmann et al., 2000, Samsonov & d'Oreye, 2012; Samsonov et al., 2020). In the Syahoo diapir, in the southeastern part of the Zagros fold and thrust belt, InSAR-derived observations showed an average ~25 mm/yr line of sight (LOS) uplift rate which was regulated by wet and dry seasons (Aftabi et al., 2010). The orogen wide constructed InSAR time series have detected 20 active salt diapirs across the Zagros that show a rate of 10-20 mm/year in the LOS direction of the satellite (Barnhart & Lohman, 2012). Anguru salt diapir is one of the salt diapirs that shows ~ 14-26 mm/yr displacement in the LOS direction of the satellite through ASAR and ALOS images from 2003 to 2010 (Ghassemi & Roustaei, 2021), the smilare study on Shah-Gheib salt diapir shows 6 mm/yr uplift and 39 mm/yr displacement in E_W direction (Shami et al.,2024) and -25-20 mm/yr in the LOS direction of the satellite for the Dashti salt diapir (Zhang et al.,2021) The Kuqa fold-thrust belt in NW China contains active namakiers which displaced up to ~25 mm/yr vertically and up to ~45 mm/yr horizontally from 2014 to 2020 (Chang et al., 2022; Colón et al., 2016; Li et al., 2014). The main cause of the movement in these namakiers is topography which controls gravity spreading, while weather variables play a minor role (Chang et al., 2023).

Zagros Fold-Thrust belt is well known for its spectacular extrusive salt diapirs (Ala, 1974; Edgel, 1996) which are scattered throughout the domain where Hormuz basal salt and Fars Salt are present (Talbot & Alavi,1996; Falcon ,1987; Hassanpour et al.,2021). It appears that diapir distribution in the Bandar Abbas and Larestan regions is denser and correlates closely with the thickness variations of the Hormuz salt Formation and also the structural elements of the area (Hessami et al., 2000, Hessami et al., 2017, Jahani et al., 2008 and 2010). Here we choose the Mazaayjan Namakier (MZJ) in the Larestan region as a target for investigating the salt glacier kinematics, this salt glacier also called Shah Gheib which refers to a place where, according to Shiite beliefs, the twelfth Imam, has set foot and is considered as a holly place, The etymology

of the word "Mazaayjan" shows that it consists of three parts: The prefix "مَ-"(Ma-) negates all of the verbs , the verb "زای" Zây meaning "give birth" and suffix گان/جان(-gân/ jân) meaning "place of" ,therefor the word Mazaayjaan meaning is a place where nothing born and it really suits the harsh nature of the region, where nothing grows due to the spread of salt in the water and soil.

The arid climate, scarce vegetation, and flat surrounding region alongside vigorous topography of MZJ make it an excellent candidate to study extrusive salt structures. The assessment of the present activity and controlling parameters of this namakier can provide constraints for their kinematic path and response to surficial processes , also can help us mitigate dangers that threaten the human population or exploit them as engineering material or a host for storage of the hydrocarbon resources.

This study, in the first step, investigated the topographic and geomorphic characteristics of the MZJ, then the Persistent scatterer (PS) method was used to construct the InSAR time series (Hooper et al., 2004; Hooper et al., 2008) of Sentinel 1-A images in ascending and descending orbits. Then the horizontal (east-west) and vertical displacement of the namakier surface has been resolved. Finally, the statistical relation between observed displacement, weather local records, and surface properties were analyzed to set constraints on factors that control the present activity and morphology of the namakier.

Geological setting

The Zagros orogenic belt extends for ~ 1800 km from Northern Iraq in the west to the Minab-Zendan Fault in the east. It is subdivided into tectonostratigraphic zones, from NE to SW, including the Sanandaj-Sirjan zone, High Zagros, the Simply Folded Belt and the Zagros foreland basin (Alavi, 1994) (Fig.1). The orogeny is the result of the collision between Arabia and Central Iran microcontinent, dated between the Late Cretaceous to Pliocene (e.g., Berberian & Berberian, 1981; Agard et al., 2005; Mouthereau, 2012; Madanipour et al., 2024), although recent studies suggest ~35-20 Ma which spread diachronically eastward (Barber et al., 2018; Koshnaw et al., 2019; Song et al., 2023). The collision caused to the horizontal shortening of the thick sedimentary cover and underlying crystalline basement in the form of folding, faulting, and rejuvenation of pre-existing salt diapirs (Hessami et al., 2001; Sherkati et al., 2005). The long-term shortening amount across the belt varies from ~ 50-70 km in the NW, ~50-65 km in the central Zagros, and ~45 km in the SE termination (Mouthereau et al., 2012) which occurred first in the form of thin-skinned deformation and then the basement involved deformation (Molinaro et al., 2005).

Present day shortening across the belt varies between ~5-9 mm/yr from NW to SE (Hessami et al., 2006; Vernant et al., 2004) and is now concentrated in the front of the belt (Oveisi et al., 2009) and mostly absorbed aseismically (Barnhart and Lohman, 2013). Growth strata throughout the belt showed that folding began around ~26-21 Ma near the Zagros Suture (Pirouz et al., 2017), ~15-11 Ma near the High Zagros in the northwest (Emami et al., 2008; Khadivi et al., 2010) and propagated sequentially toward SE, reached the Simply folded Belt in ~6-4 Ma (Ruh et al., 2014; Najafi et al., 2019). Along the folding, salt diapirs are another important feature of the Zagros FTB. They include about 200 emergent salt diapirs have been identified throughout the belt (Jahani et al., 2009), which originated from two evaporitic horizons: the Neoproterozoic-Cambrian Hormuz Salt and the late Oligocene-early Miocene Fars salt (Bahroudi and Koyi, 2004). The Hormuz basal series acts as the main detachment horizon separating the Phanerozoic sedimentary cover from the Arabian crystalline basement (Bahroudi and Koyi, 2004; Sherkati et al., 2006).

The timing of the salt movement is controversial; some authors related the onset of salt movement to the Cretaceous Neotethys subduction and emplacement of ophiolites

(Harison,1930; Huerford et al.,1984; Talbot and Alavi,1996), although others showed based on growth starats, local unconformities, and reworked Hormuz materials that Hormuz salt started to raising after deposition (Motie,1995; Sherkati and Letouzey, 2004; Jahani et al., 2009; Motamedi et al., 2011; Perroti et al., 2016; Snidero et al., 2020, Taghikhani et al., 2024).

The salt structure currently can be seen in association with different structures, from the culmination of anticlines, and depression of synclines as well as along the thrusts and tear faults (Talbot and Alavi, 1996; Jahani et al., 2007). It has been suggested that some of the salt diapirs raised reactively in response to the opening of pull-apart structures along the strike-slip faults (Talbot and Alavi, 1996; Hessami et al., 2001). However, some studies documented salt diapirs as down-built pre-existing diapirs which squeezed and rejuvenated during shortening (Sherkati and Letouzey, 2004; Jahani et al., 2009). MZJ is an active subaerial salt diapir cut the eastern nose of the Gach and MZJ anticlines on the way between Bandar Abbas and Laristan in the Fars province (Fig. 2). The MZJ is morphologically classified as an active type B diapir (Jahani et al., 2007), which has a kidney-like shape at the surface, with a maximum diameter of ~14 km in the N-S direction and a minimum diameter of 8 km in the E-W direction (Fig. 2). Its circumference and area are 41500 m and 107693 m^2, respectively (Fig.2). The Diapir has a central circular fountain at the surface with a diameter of ~ 2 km, probably rising above a feeding vent, and a summit elevation of ~1370 m above sea level surrounded by overhanging namakiers. The Namakier has ~800 m mean elevation above sea level and ~200 meter higher than the neighboring plain.

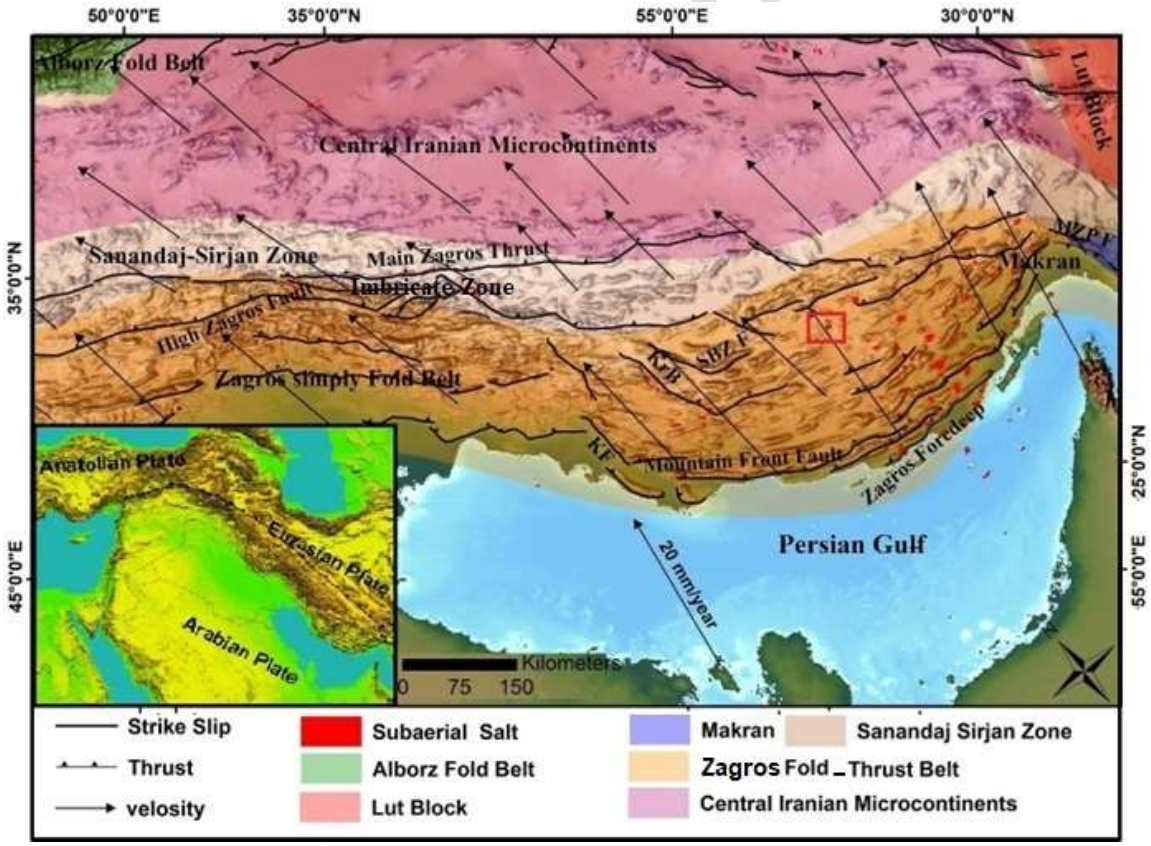

Figure 1. Geological map of Iran, showing the main tectonic subdivisions including the Zagros Fold-and-Trust Belt, the Sanandaj-Sirjan Zone, Central Iran Microcontinent, Makran, Alborz Fold Belt and Lut Block. The black arrows show GPS horizontal velocity vectors respect to fixed Eurasia (Khorami et al., 2019). The red rectangle shows the study area. The abbreviations for faults are KF: Kazeroun , KrB: Karebas , SBZ: Sabzpoushan

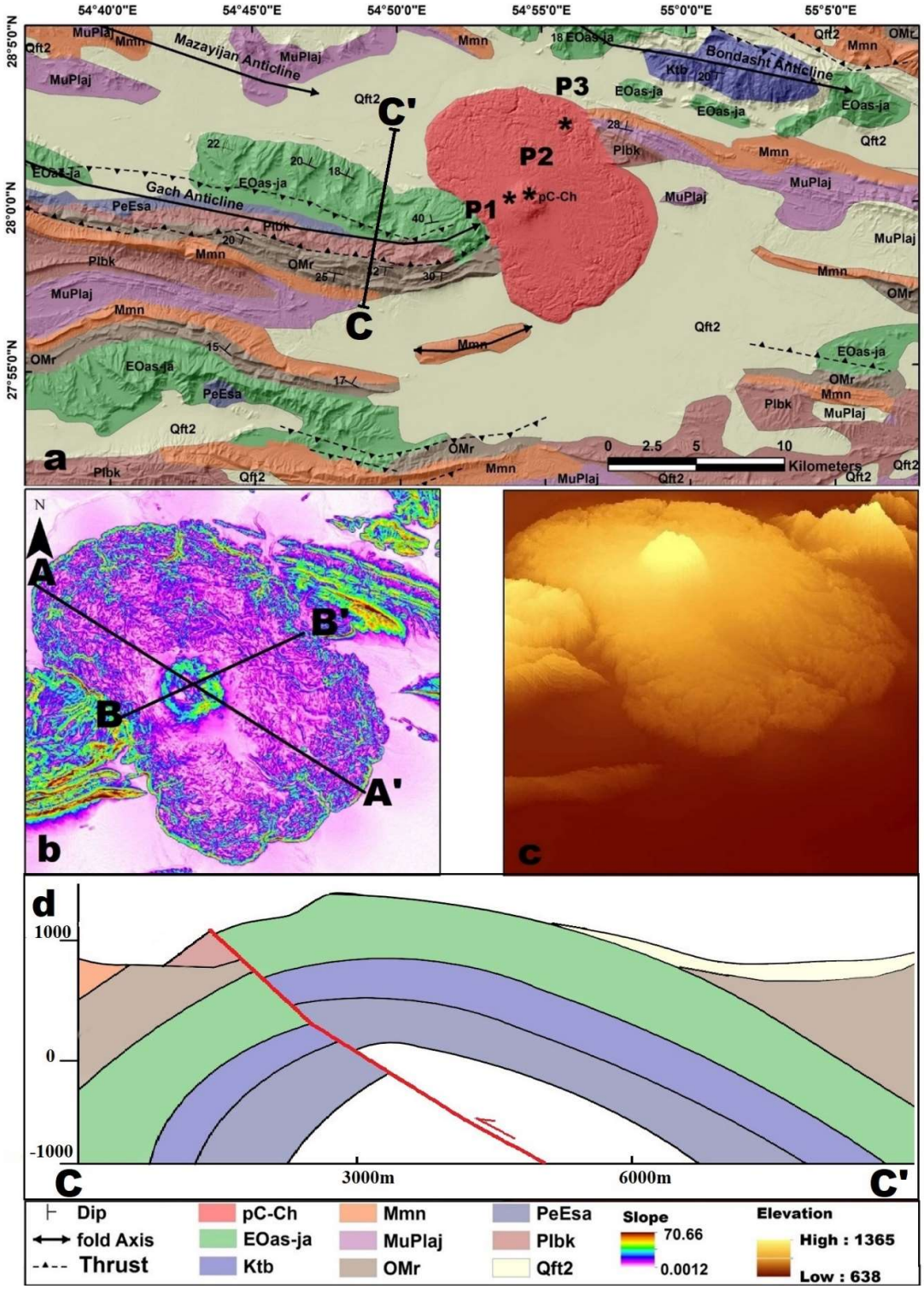

Figure 2. a) Simplified geologic map of the study area over lied on the shaded relief map, the lithostratigraphic units include Qft2: Quaternary alluvium, Plbk: Pliocene Bakhtiari Formation, MuPlaj: Miocene Aghajari Formation, Mmn: Miocene Mishan formation, OMr: Oligocene-Moicene Razak formation, EOas-ja: Eocene-Oligocene Asmari-Jahrum Formation, Ktb: Kretaceous Tarbur formation, PeEsa: Paleocene Eocene Sachun formation, pC-Ch: Precambrian Hormuz Series; Points 1-3 present location of the selected pixels that their time series are shown in Fig. 7. b) Slope map of the MZJ. A-A' and B-B' show the path of topography-slope profiles. C) 3D topography model of MZJ.d)geological cross section across the gach anticline C-C'

The MZJ diapir extruded on the near-flat surface and spread freely in a radial direction until has reached the neighboring highlands. The main body of the dome consisted of dirty evaporites including halite, gypsum, and reddish shales Metamorphosed sedimentary rocks in association with exotic igneous fragments can be seen in some parts of the glacier.

The namakier is surrounded by the Gach and Mazayijan anticline in the east and Bandubast anticline in the north (Fig. 2). The heights of Asmari limestones, Aghajari sandstones, and Gachsaran evaporites limit glacier further spreading in the east-west direction and caused to form a kidney_like shape in glacier (Fig. 2).

The region experiences a minimum temperature of 20^{o}C in the wet seasons (autumn and winter) and a maximum temperature 50^{o}C in the arid seasons (spring and summer). The average annual precipitation is ~ 200 mm and most of it is a sparse flash rain occurring from October to April. The study period was selected in a such way that started by the wet season and was followed by arid season.

Methodology

Radar is an advanced remote sensing technique that, unlike methods such as GPS and surveying, which focus on measuring at one point, provides earth surface deformation with wide coverage, and appropriate accuracy while operating at different times and weather conditions (Hooper et al., 2012). The SAR interferometry relies on measuring the phase difference between two SAR images, acquired from different orbital positions and at various times for the same area.

The interferometric phase ($\Delta\varphi_{int}$) is combination of deformation phase (φ_{def}), flat earth phase (φ_{flat}), topography phase and noise phase (φ_{noise}):

$$\Delta\varphi_{int} = \varphi_{def} + \varphi_{topo} + \varphi_{flat} + \varphi_{noise} \quad (1)$$

To track the temporal evolution of the earth surface through InSAR observations, we need to construct timeseries but unfortunately InSAR time series inherently suffer from temporal decorrelation of phase resulting from the different contributions of scatterers present in a resolution cell between different satellite passes (Hooper et al., 2012). To overcome this limitation, approaches such as Small Baseline Subset (SBAS) (Berardino et al., 2002) and Persistent/Permanent Scatterer (PS) have been proposed (Feretti et al., 2001; Hooper et al., 2004). PS algorithms work with a series of interferograms all formed with reference to a single "master" SAR image, and rely on identifying resolution elements in which the echo from a single scatterer dominates (Ferretti et al., 2001; Hooper et al., 2004). The Stanford method for Persistent Scatterer interferometry, introduced by Hooper et al. (2004), does not require a specific temporal model for deformation and is more suitable for phenomena that exhibit low linearity in time and areas where man-made structures are rare (Hooper et al., 2012). Therefore, it will be a suitable method for studying subaerial salt diapirs surface displacements.

This study used the Sentinel Application Platform (SNAP) to produce stacks of single master interferograms from Sentinel 1-A SLC IW TOPS mode images and StaMPS for time series construction based on the PS algorithm (Hooper et al., 2007, 2008). Snap2stamps python scripts has employed to automatize and wrapping IFGs for subsequent PS processing, (Delgado et al., 2019).

Precise orbit files and enhanced spectral diversity applied for coregistration (Scheiber & Moreira, 1999) and 1-arcsec Shuttle Radar Topography Mission (SRTM) Digital Elevation Model (DEM) (Farr and Kobrick, 2000) used for removing topographic phase from IFGs. After the final PS points selection based on StaMPS procedure, the final phase was unwrapped three dimensionally (Hooper and Zebker, 2007), atmospheric phase screen was mitigated using Toolbox for Reducing Atmospheric InSAR Noise (TRAIN) (Bekaert et al., 2015), and the ECMWF Reanalysis v5 (ERA-5) weather model (Hersbach et al., 2020).

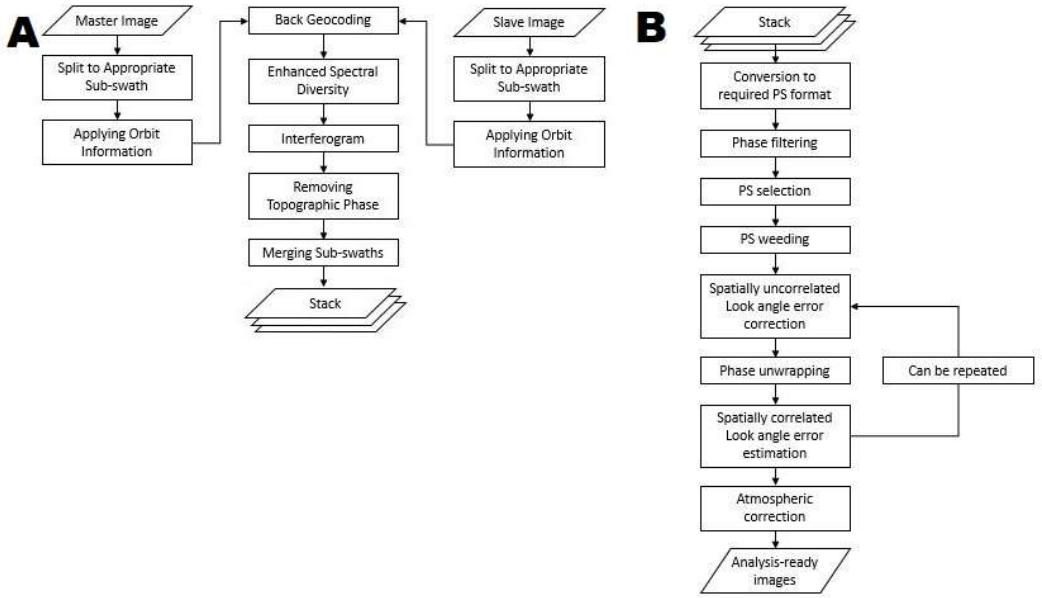

Figure 3. flowchart of processing steps for creating IFGs Stack (A) and extracting PS points timeseries in the StaMPS software (B)

The entire process is performed for ascending and descending orbits and the average displacement rate in the line-of-sight direction is extracted, by combining results from two orbits in the following equation the displacements in the LOS directions decomposed into the vertical and horizontal (east-west) components; because of near polar orbits of radar satelites , the SAR images has minimum sensitivity to the N_S component of horizontal movements (Samieie-Esfahany et al., 2009).

$$\begin{pmatrix} V_{asc} \\ V_{dsc} \end{pmatrix} = \begin{pmatrix} -sin\theta_{asc}cos\alpha_{asc} & cos\theta_{asc} \\ -sin\theta_{dsc}cos\alpha_{dsc} & cos\theta_{dsc} \end{pmatrix} \begin{pmatrix} V_e \\ V_u \end{pmatrix} \quad (2)$$

In the above equation, θ is the incidence angle and α is azimuth. V_{asc}, V_{dsc}, V_e, and V_u are velocity vectors of ascending geometry, descending geometry, east-west direction, and up-down direction, respectively (Hansen, 2001; Fuhrmann & Garthwaite, 2019).

To validate the accuracy of velocity maps, we have calculated the Standard Deviation(SD) of velocity for all extracted PS points timeseries based on the equation :

$$\sigma = \sqrt{\frac{1}{N}\sum_N^i (v_i - \bar{v})} \quad (3)$$

N is a number of PS points, v_i is velocity vector for each PS point and $\bar{v}$ is mean velocity of all points.

To assess the accuracy of predicted displacement time series for selected points we have calculated the R- Squared(R^2) values for each fitted displacement curve according to:

$$R^2 = 1 - \frac{\sum(v_i - \hat{v})}{\sum(v_i - \bar{v})} \quad (4)$$

$\hat{v}$ is predicted values for velocity by curve fitting.

Datasets

In this study Sentinel-1 Single Look Complex (downloaded from Alaska Satellite Facility) images acquired in the Interferometric wide-swath (IW) beam mode and VV polarization were processed for 34 images in ascending orbit (table.1, supplementary material) (path 112 and frame 587) and 36 images in descending orbit (table.2, supplementary material) (path 110 and frame

235), resolution of images is 5 × 20 m (range × azimuth) and covering three hydrologic year from September 2014 to September 2017. All SLC images and correspondent POD Precise Orbit Ephemerides, obtained from the Alaska Satellite Facility (ASF), the Shuttle Radar Topographic Mission (SRTM) digital elevation model (DEM) (from https://srtm.csi.cgiar.org/srtmdata/) with a pixel resolution of 1 arc second (Farr & Kobrick, 2000) were used for topographic phase removal and geomorphic features extraction, the weather records include daily temperature and precipitation for nearest station located in 25.578° N and 54.864° E in 18 Km distance from the MZJ acquired from the Iran Weather Organization through proposal submission.

Results

In this study, 34 and 36 SLC images in the ascending (ASC) and descending (DSC) tracks from September 2014 to September 2017 have been processed to produce line-of-sight (LOS) mean velocity maps. The results are illustrated in Fig. 6a and b. The entire body of the MZJ diapir exhibits good coherence, then the surface deformation was captured well, except for regions affected by layover and shadowing around the central dome or by high erosion/dissolution rate zones along the drainage tributaries.

Table 1. Pairwise correlation table of selected point's vertical and horizontal displacement to each other and also concerning precipitation and temperature.

Time series	Vertical 1	Vertical 2	Vertical 3	E-W1	E-W2	E-W3	Temperature	Precipitation
Vertical 1	1.00	0.47	0.71	-0.79	-0.82	-0.53	-0.30	0.30
Vertical 2	0.47	1.00	0.59	-0.73	-0.19	-0.73	-0.19	0.48
Vertical 3	0.71	0.59	1.00	-0.68	-0.62	-0.80	-0.36	0.53
E-W1	-0.79	-0.73	-0.68	1.00	0.64	0.69	0.28	-0.33
E-W2	-0.82	-0.19	-0.62	0.64	1.00	0.37	0.33	-0.16
E-W3	-0.53	-0.73	-0.80	0.69	0.37	1.00	0.13	-0.42
Temperature	-0.30	-0.19	-0.36	0.28	0.33	0.13	1.00	-0.57
Precipitation	0.30	0.48	0.53	-0.33	-0.16	-0.42	-0.57	1.00

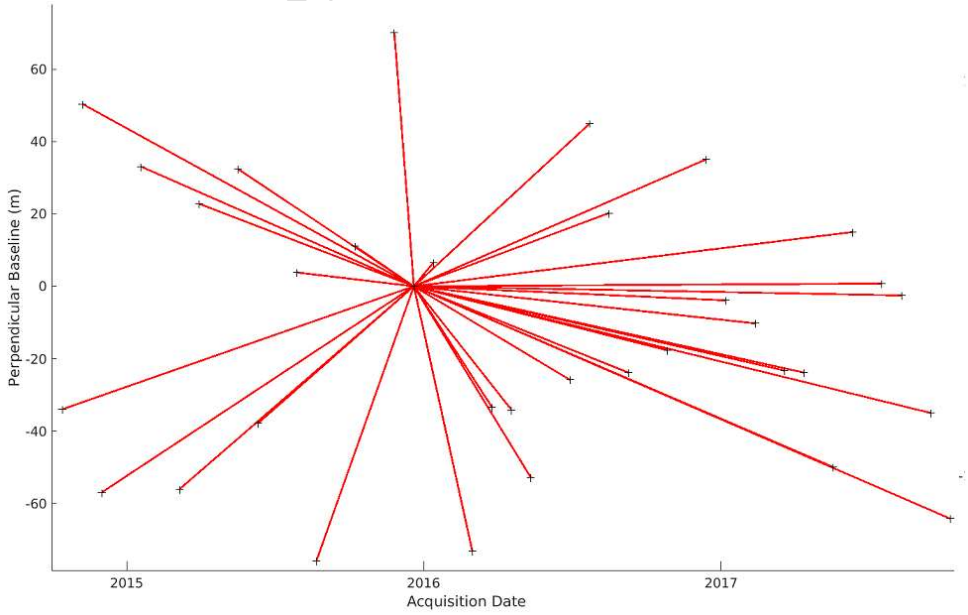

Figure 4. Baseline plot for ascending orbit. The vertical axis shows the perpendicular baseline in meter and the horizontal axis shows the acquisition date, The black plus (+) presents for each SLC image

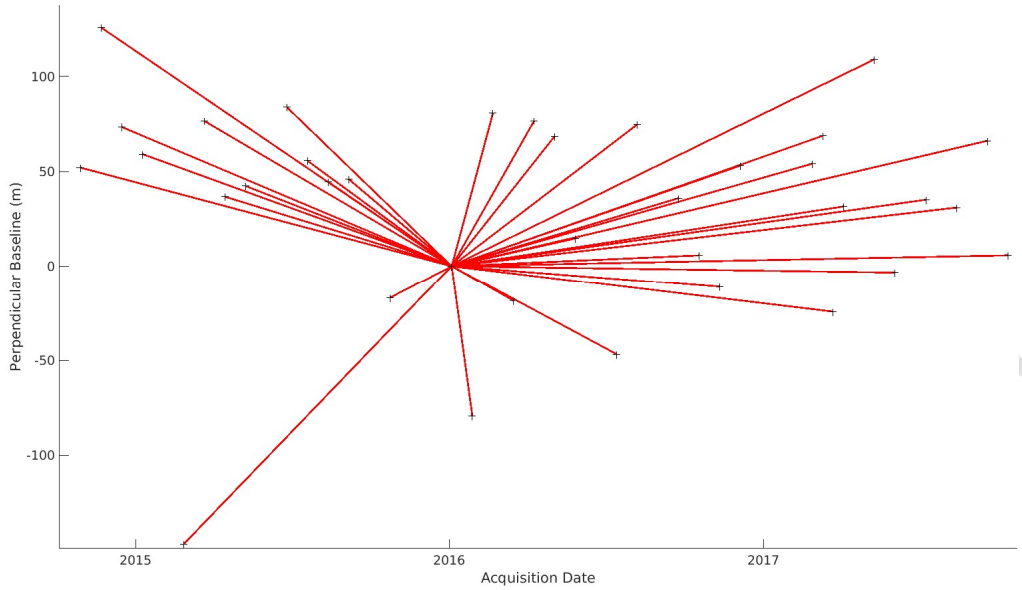

Figure 5. Baseline plot for ascending orbit. The vertical axis shows the perpendicular baseline in meter and the horizontal axis shows the acquisition date. The black plus (+) presents for each SLC image

The resulted SD maps for ascending track shows a range of 0.3_1.8 mm/yr which indicate good coherency and low discrepancy for extracted velocity values, for descending track the SD varies between 0.3_1.7 mm/yr. For both tracks, maximum SD was observed for the central dome, which indicates high activity in the form of uplift and subsidence in this region (Fig.1a and b, supplementary material).

The yellow color in the map (positive values) shows motion toward the satellite and the blue color (negative values) shows motion away from the satellite (Fig. 6a and b). Both tracks show three distinct lobed patterns of line-of-sight (LOS) displacement formed around the central dome and separated by regions of lower movement. In the ascending track (Fig. 6a), the western lobe in yellow has moved toward the satellite at a maximum rate of ~15 mm/year, while other lobes in the north-northeastern and southeastern parts have moved at a maximum rate of ~25 mm/year away from the satellite. The same three lobes show a reversed displacement direction in the descending tracks which is due to a significant contribution of the horizontal component in the LOS displacement.

The horizontal E-W and vertical annual displacement rates have documented the activity of the MZJ diapir (Fig. 6). The blue colors (positive values) indicate westward displacement and uplift, while the red colors (negative values) indicate eastward displacement and subsidence. As mentioned earlier, the MZJ shows significant horizontal displacement, which can be seen as a lobed pattern in Fig. 6a. The northwestern lobe displaced toward the west at the maximum rate of ~25 mm/year, and the lobes in the northeast and southeast moved eastward at a rate of ~35 mm/year. The maximum horizontal deformation concentrated at the central dome where three asymmetric lobes meet, and gradually decreased toward the Namakier margins. The vertical displacement coincided mainly with the central dome (Fig. 6b). The maximum uplift of ~15 mm/year and the maximum subsidence of ~23 mm/year was observed at the northern parts of the central dome while other parts of the MZJ showed only small vertical displacements that disappeared toward the namkier`s margins.

To describe the distribution of surface velocity, slope and elevation as well as the vertical and horizontal displacement rate variations of the MZJ diapir have been plotted against the topography and slope of the area along the A-A′ and B-B′ profiles (Figs. 8 and 9).

Profile A-A′ has constructed in an NW-SE direction (Fig. 2b) to cross two opposite lobes of

horizontal displacement (Fig. 8). An abrupt increase in elevation occurred and coincidently a westward movement and the slope is increased where the profile path reached the salt apron (Fig. 8). The elevation of the salt diapir is gradually increased while the slopes became gentler (Fig. 8). This caused the displacement rate to decrease while remaining positive, this trend continued on the salt apron until the profile reached the central dome where the maximum elevation and slope occurred and consequently, the maximum displacement rates recorded. The positive values of displacement and westward movement of the salt surface have been maintained to the middle of the central dome. However, the displacement direction of the salt surface changed when the slope shifted toward the east.

The horizontal displacement direction of the salt surface has changed in the southeastern flanks of the dome again to a maximum value where the elevation decreases and the maximum slope causes an abrupt increase in eastward movement. The displacement rates also decrease, although they continue to remain negative towards the east, after the central dome where the slope is gentler.

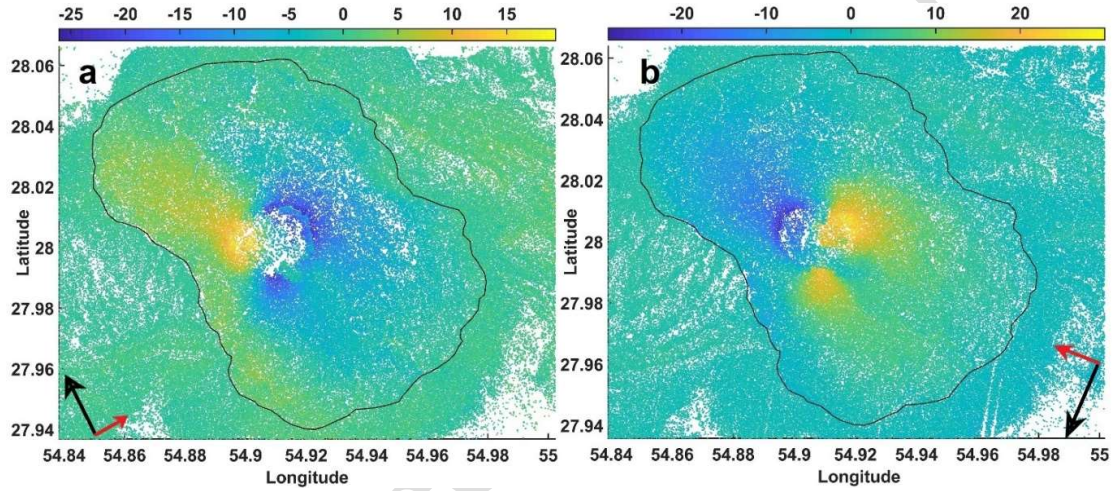

Figure 6. Annual mean LOS displacement map (values are in mm per year) for ascending (a) and descending tracks (b). The yellow colors (positive values) show motion toward the satellite and the blue colors (negative values) show motion away from the satellite. The black line shows the MZJ extent

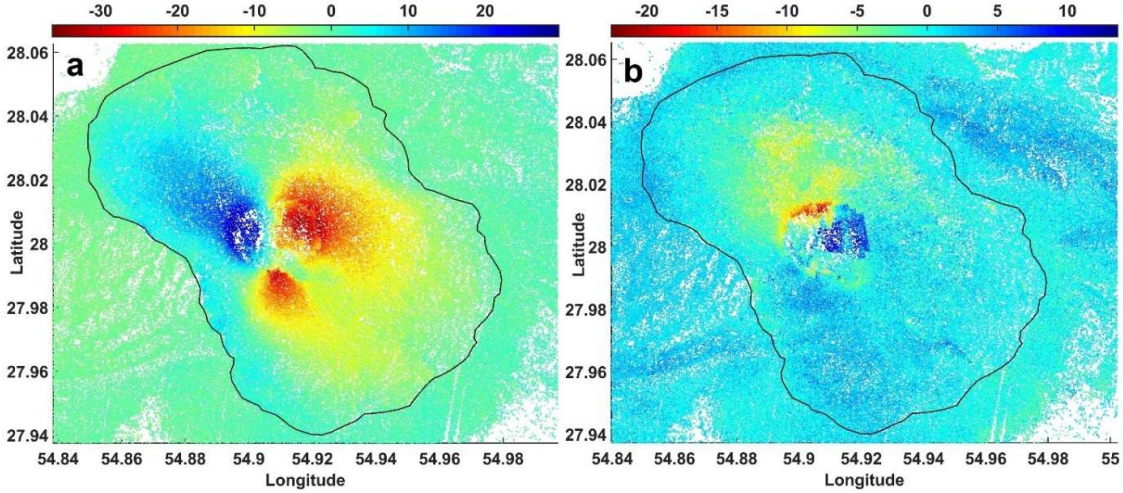

Figure 7. Horizontal E-W (a) and vertical (b) components of annual mean displacement rates in the MZJ salt diapir (values are in mm per year). The blue colors (positive values) show westward and uplift displacement while the red colors (negative values) show eastward and subsidence displacement, black line shows the MZJ extent

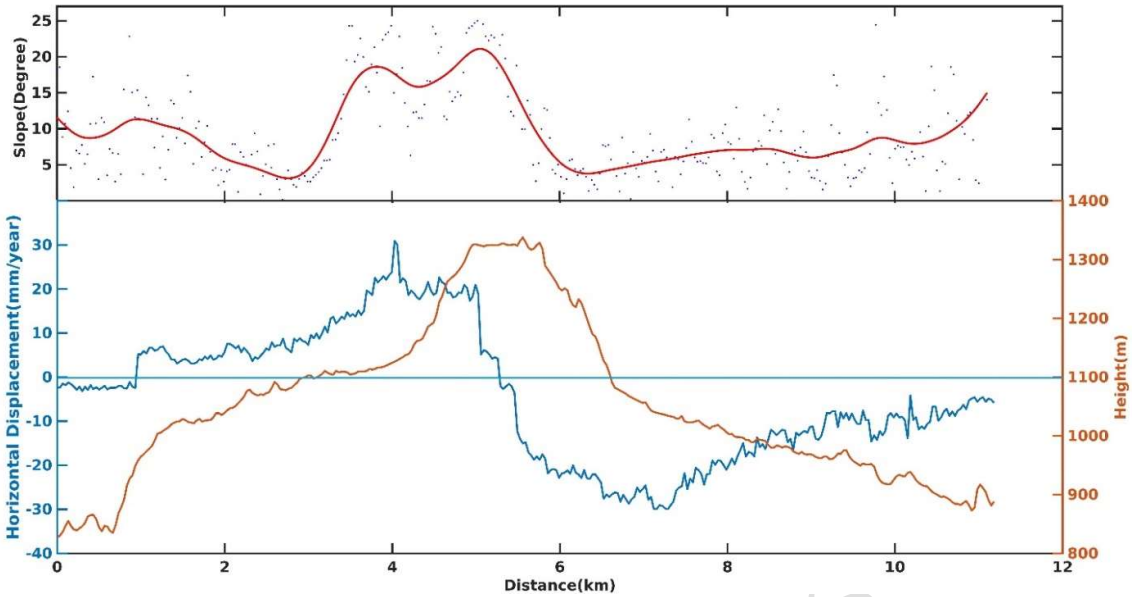

Figure 8. Variation of horizontal displacement rate, topography, and slope along the profile A-A′ (left-right). the blue curve corresponds to the displacement rate (the positive and negative values correspond to westward and eastward movements respectively), the brown curve corresponds to topography, and the red curve presents the slope

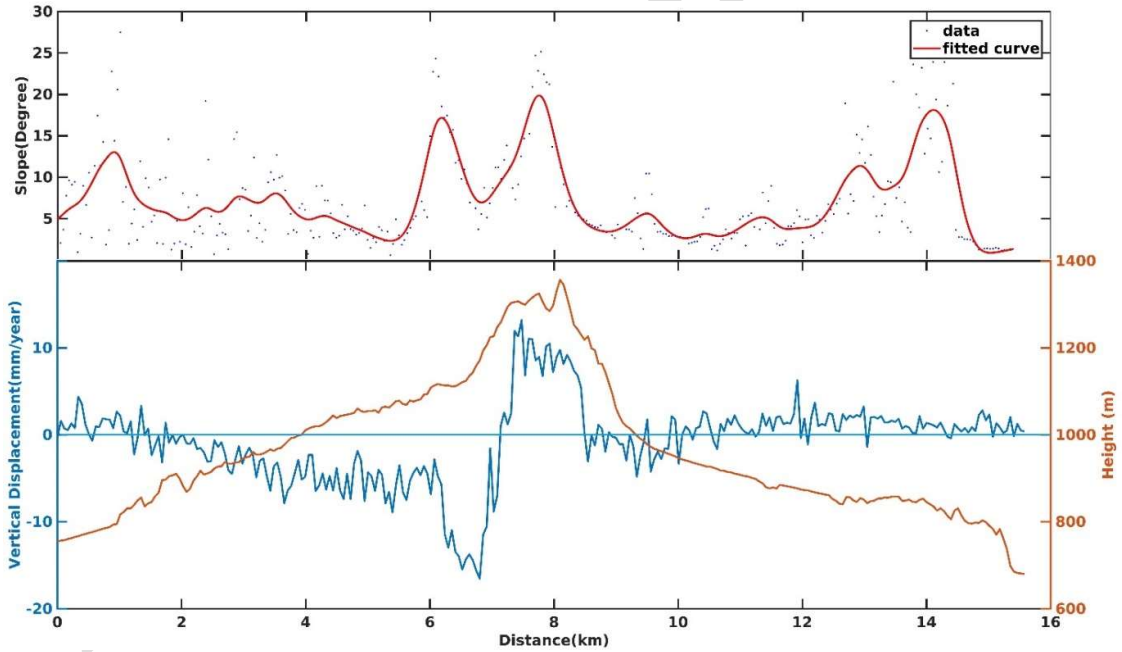

Figure 9. Variation of the vertical displacement rate, topography, and slope along the profile B-B′ (left-right), the blue curve corresponding to displacement rate (the positive and negative values correspond to uplift and subsidence respectively), the brown curve corresponding to topography and the red curve is for slope

Taken together, the absolute values of the horizontal displacement rate of salt diapir show a strong correlation with the elevation, then, the elevation (the thickness of the salt), steepness and slope direction mainly control the salt horizontal displacement rate and direction.

Profile B-B′ has been constructed in the W-E direction to present the observed vertical displacement of the salt surface, which crosses two contrasting zones of subsidence in the west

and uplift in the east (Fig. 2b). The elevation and slope have increased by the thickness of the salt in the salt apron (Fig. 9). This led to an increase in the slope and surface subsidence (Fig. 9). The observed subsidence rate constantly increased until the profile reached the central dome and due to the abrupt increase in elevation and slope, the subsidence rate increased several times (Fig 8). At the top of the central dome which has a near-flat topography, the slope decreased, but the maximum displacement rate as uplift persisted. The uplift rate has harmonically decreased with the decrease in elevation (Fig. 9).

Discussion:

Here we examine and compare the uplift rates and then constrain the internal forces that drive the salt movement. Then, the effect of the surface parameters including topography, slope, and climatic factors i.e. temperature and precipitation has been examined for the observed horizontal and vertical displacements of the salt diapir.

Internal driving forces of the salt diaper uplift rates

The uplift rates at the MZJ are similar to those previously reported for the Zagros, ranging from -10 to +10 mm/year(Barnhart & Lohman,2012), which is higher than ~4mm/yr that was measured at Qom Kuh in North Central Iran (Abdolmaleki et al., 2014), ~8 mm/year for Kalut basin in Central Iran (Mohammadnia et al., 2021), ~4.6 mm/year for Northwest Yemen (Davison et al., 1996), and ~1-6 mm/year for Qeshm and Hormuz islands near the Persian Gulf coast (Bruthan et al., 2008). However, it is lower than the ~25 mm/year rate reported for Kuqa Fold-Thrust Belt (KFTB) (Chang et al., 2023), another study using Sentinel-1 satellite data from 2016 to 2019 on the MZJ shows an uplift rate of 6 mm/year and a horizontal displacement rate of 39 mm/year in the east-west direction. This difference is due to the different time period of the data used and also the use of the SBAS algorithm to extract the displacement time series (Shami et al.,2024) on other hand the displacement rates reported for the central dome are the probabilities of machine learning, not deterministic results .

The difference between observed uplift rates can be linked to the tectonic setting in which salt diapirs reached the surface, Sedimentation, shortening, and extension rates are considered to be the main driving forces of salt extrusion (Hudec & Jackson, 2007). For example, the higher rates of salt uplift in the internal Fars Arc and KFTB can be attributed to the higher shortening/extension rates in comparison to Central Iran, and the Dead Sea. Sedimentation in the mini basins surrounding the salt diapir is one of the major mechanisms that could drive salt extrusion in the active salt diapirs. For example, in the Persian Gulf as a present-day foreland basin of the Zagros orogeny and the depocenter of sedimentation, the maximum rate of sedimentation is ~0.064 mm/yr, resulting in an uplift rate of ~0.025 mm/year for the diapirs (Perotti et al., 2016), this uplift rate is several times lesser than the observed uplift rate for subaerial salt domes in the Fars Arc (Barnhart and Lohman, 2012). The sedimentation rate around the MZJ diapir is restricted to active fluvial sediments that cannot exert enough force for the observed salt diaper uplift rate. Therefore, as indicated by previous studies the squeezing of pre-existing down-built diapirs after the continental collision and shortening across the belt can be considered the main driver of salt uplift in the ZFTB (Talbot and Alavi, 1996; Sherkati et al., 2004). GPS measurements indicated that the convergence of Arabia and Central Iran persists and is accommodated by active folding, diapirism, and faulting (Khorrami et al., 2019).

Effect of the topography on the surface displacement of salt diapir

The observed positive spatial correlation between elevation and surface displacements suggests

that zones with higher elevation and consequently higher gravitational potential energy are more susceptible to gravitational spreading (England & McKenzie, 1982). Then it can be assumed as the main mechanism responsible for downslope movement in the form of subsidence and horizontal movement (Chang et al., 2023; Talbot & Pahjola, 2009). It is also clear that slope direction and degree control the horizontal movement direction and rate; the correlation between active uplift of the salt diapir and elevation is different, e.g. where the salt uplift (extrusion) is higher the thickness and elevation will increase, in other words, salt extrusion rate control the elevation in contradiction to what observed about horizontal movement rate. It is also evident that the uplifting zone, due to its weight, simultaneously subsided. However, the net results appeared as an uplift. In other words, the actual amount of uplift is greater because a portion of extruded salt spreads downslope before it can be captured by SAR images, The results of machine learning also show that the topographic layer as the initial input data can predict spatial changes in the surface displacement of the salt flat with the lowest error rate (Shami et al., 2024).

Effect of the precipitation on the temporal and spatial distribution of the salt diapir displacement

To investigate the temporal and spatial distribution of the vertical and horizontal displacement, three points were selected. They are located on the contrasting zones of displacement (Fig. 2a). The point`s temporal evolutions are illustrated in Figures 7 and 8, showing the cumulative displacement and the precipitation against time. There was a low correlation in statistical comparison to the denser displacement time series due to the scarce rainfall in the study area. However, visual similarities were noticeable; the visual inspection of time series has been employed successfully for the comparison and classification of groundwater head data (Haaf & Barthel, 2018; Barthel et Al., 2022), rainfall (Muchuru et al., 2015), stream flow (Strohmenger et al., 2023).

The precipitation time series can be divided into three different seasons. Almost the wet season began between December 2014 and March 2015. The dry season between March 2015 to February 2016, and a major wet season from February 2016 until the end of the period (Fig 9 and 10). The course of heavy rainfall from March -April 2017 occurred in the middle of this period (Figs. 9 and 10).

The time series of point 1, which is located in the northwestern lobe of the horizontal displacement map and high elevation of the central dome (Fig. 2a), began in October with an eastward movement (Fig. 7).

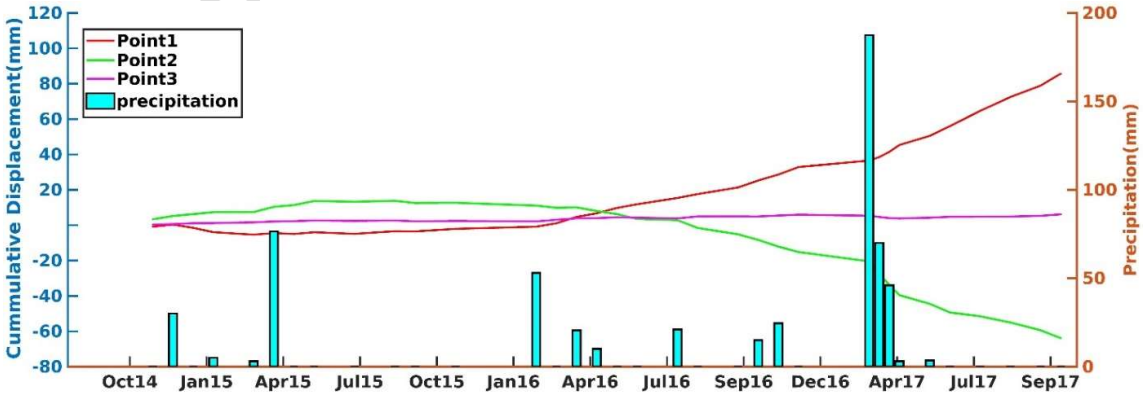

Figure 10. Horizontal displacement time series of selected points 1 to 3 on the MZJ surface. The left and right vertical axes show displacement and precipitation, respectively. Positive values of displacement correspond to the westward movement and negative values correspond to the eastward movement

This movement continued until April 2015, when significant rainfall occurred (~75 mm). Thereafter, the point began its gradual westward movement, which was coincided with a long dry period and interrupted by rainfall in January 2016, when simultaneously an abrupt increase in displacement rate occurred. The point maintained its westward movement throughout the period and even experienced its maximum acceleration after the prolonged and heavy rainfall in March and April 2017 (~350 mm). In general, it can be concluded that the northwestern lobe, except at the beginning of the movement, which shrank towards the east, expanded continuously to the west and shows a good correlation with rainfall events.

Point 2 which is located in the Northeastern lobe on the central dome summit (Fig. 2a) started its slow shrinkage toward the west which continued until May 2015 at the beginning of the time series (Fig. 9). Then, the direction reversed and the point expanded toward the east which was maintained until the end of the period. The point movements are not uniform and show some irregularities that have not coincided exactly with the rainfall events but generally in dry season shows limited movement and in wet seasons, especially in the rare case of March and April 2017 increased several times.

The time series of Point 3 (Fig. 2a), located at the rim of the northeastern lobe where the salt apron has minimum thickness shows negligible displacement except for heavy rainfall in March and April 2017 which correlates with a clear increase in its eastward movement.

In summary, the rate and direction of horizontal movement are regulated by wet and dry seasons. This dependency and back-and-forth movements have been previously reported in several cases all around the world including the Kuh-e-Namak Dashti (Talbot & Rogers, 1980; Zhang et al., 2021), Kuhe Jahani (Talbot et al., 2000) Siyahoo (Aftabi et al., 2010), Western Kuqa Fold-Thrust Belt (Chang et al., 2023). Microstructural studies indicate that the presence of a small amount of moisture decreased the salt creep strength dramatically and weakened it at low-stress rates. Therefore in the wet seasons, infiltration of meteoric waters weakened the salt rocks and consequently enhanced their gravitational spreading (Spiers et al., 1986; Urai et al., 1986).

The vertical displacement of the marker points has also been investigated during the observation time span (Fig. 10). Displacement of point 1 started with subside and then it's the subsidence rate decreased between April 2015 and January 2016. This has been correlated with the dry time span, in a wet period between January 2016 and September 2016. The subsidence rate is accelerated again with the maximum amount after the March and April 2017 heavy and prolonged rainfalls. In general, it is clear that point 1 subsidence shows a good correlation with the precipitation.

Point 2, which is located in the uplifting zone of the central dome is generally uplifting. However, it has experienced some abrupt increase in uplift rate. There is a correlation between precipitation and uplift rate in point 3 which is located at the low-elevation periphery of the salt apron, except for April, and March 2017.

It can be proposed that the uplift and subsidence show different responses to the precipitation. The subsidence is regulated by wet and dry seasons because subsidence is the direct consequence of horizontal movement which itself depends on the moisture content of salt rocks. While uplift is the result of salt extrusion due to internal forces. It is worth noting that the rate of salt extrusion from the orifice is influenced by the balance between internal forces and the weight and strength of salt rocks against the flow. Then, the occurrence of rainfall by increasing moisture content and weakening the salt body on one hand and unloading by erosion, dissolution, and gravity spreading above the orifice on the other hand caused to internal forces overcome the resisting forces and more salt extrudes to the surface (Dooley et al., 2009; Słotwiński et al., 2023).

Precipitation plays an important role in the dissolution and erosion of salt rocks inherently by changing surface geometry (Talbot et al., 2000; Zarei et al., 2014). This could lead to reduced

backscattering of radar echoes and cause coherency loss. Then, the surface area of the salt diapirs that experienced erosion will not be efficiently identified and recorded by the InSAR time series.

The effect of the weather temperature variation and salt movements

The weather temperature data from the station near MZJ shows a strong seasonal pattern, with maximum and minimum temperatures of about 44°C and 18°C recorded in July (summer) and January (winter), respectively. To clarify the role of temperature changes on the observed displacement pattern, the time series was decomposed, linear trends were removed, and only seasonal components were preserved. Finally, the seasonal components were compared to the temperature time series of the study region (Fig. 12).

The displacement time series of two points located in the contrasting zones of uplift/subsidence and eastward/westward movement have been plotted against temperature variations (Figs 12a, b). It is deduced from the graph that Point 1 has uplift by decreasing the temperature and then subsided by increasing temperature (Fig. 9a). The uplift of Point 1 was harmonical during July 2015, when it experienced the highest weather temperature (Fig. 12a). However, this harmony and confliction between Point 1 displacement and the weather temperature have changed several times (Fig. 12a). Then, it is difficult to establish a specific pattern between salt diapir displacement and the weather temperature.

The horizontal movement of Point 1 started to move eastward (shrunk) by decreasing temperature in winter and gradually moved toward the west (expansion) (Fig. 12a). However, this pattern has not continued and the point moved toward the east while the temperature still increased (Fig. 12a). On the other hand, the horizontal displacement of the point does not correlate with temperature changes like the vertical displacement (Fig. 12a). The time series of Point 2 which is located in the northeastern uplifting zone of MZJ, also does not show any evidence of displacement/weather temperature correlation (Fig. 12b).

To better understand the relationship between the displacement of selected points (horizontal and vertical) and surficial parameters (temperature and precipitation), the correlation between each pair is calculated and depicted in Table 1. According to the 8th column of the table, the absolute values of correlation between displacement components of all points and the temperature are lower than 0.37 which indicates there is a weak relation between the two parameters in the study period. It can be concluded that the effect of temperature in comparison to other parameters is negligible. , This was also previously reported for Kuh-e-Namak Dashti in the SE Zagros (Zhang et al., 2021) and Western Kuqa Fold-Thrust Belt (Chang et al., 2023).

The relation between displacement components of points:

Generally, Point 1 on the MZJ salt diapir shrinks toward the east during uplifting and, expands toward the west when subsiding (Fig. 11a). This contrasting behavior between vertical and horizontal displacement was reversed during April 2017 rainfall. Point 2 on the MZJ salt diapir has also shown the same pattern, and the effect of exceptional rainfall of April 2017 is even stronger (Fig. 11 b). The mean value of the correlation between horizontal and vertical displacement is about -0.65 (Table 3). This contradiction indicates that gravity spreading in a down-slope direction caused horizontal and subsidence movement to occur together. Then it is expected to have accumulation and uplift of the extruded salt in the central dome of the diapir during dry seasons (very low moisture content of salt) because it can not be easily spread by the gravitational forces.

Marker Point 1 (which is located in the subsiding and westward movement zone of the diapir) and Point 2 (which is located in the uplifting and eastward movement zone of the diapir) have

the lowest correlation together. They show a good correlation with marker Point 3 which is located far from the central dome near the periphery of the salt apron (Table 1). This relation between points indicates the simultaneous effect of the main (main long-lasting deformation) and minor (seasonal effect) factors of MZJ salt diapir driving forces. This is in contradiction to the behavior of the other salt diapirs in the Zagros fold-Thrust Belt like Siyahoo and Dashti salt diapirs (Roustaei et al., 2010; Zhang et al., 2021). They represent alternate uplift and subsidence zones between the central dome and flanks during the wet and dry seasons.

Finally, aside from the strong seasonal behavior of salt kinematics, the average seasonal displacements are close to zero because the displacement values in opposite seasons neutralize each other (point 3 in Figs 7 and 8). The present-day morphology of MZJ salt diapir is formed by competing tectonics uplift of the diapir and destructive gravity spreading processes.

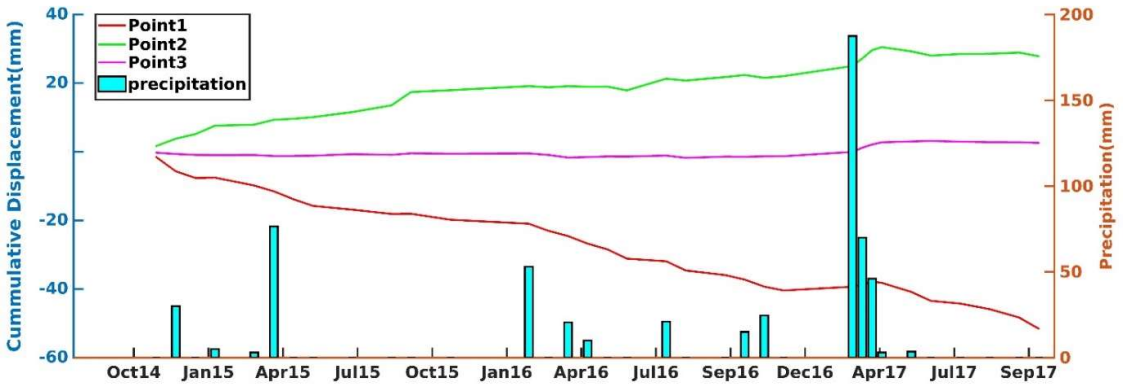

Figure 11. Vertical displacement time series of selected points 1 to 3 on the MZJ surface, the left and the right vertical axes show displacement and precipitation respectively. Positive values of displacement correspond to uplift and negative values correspond to subsidence

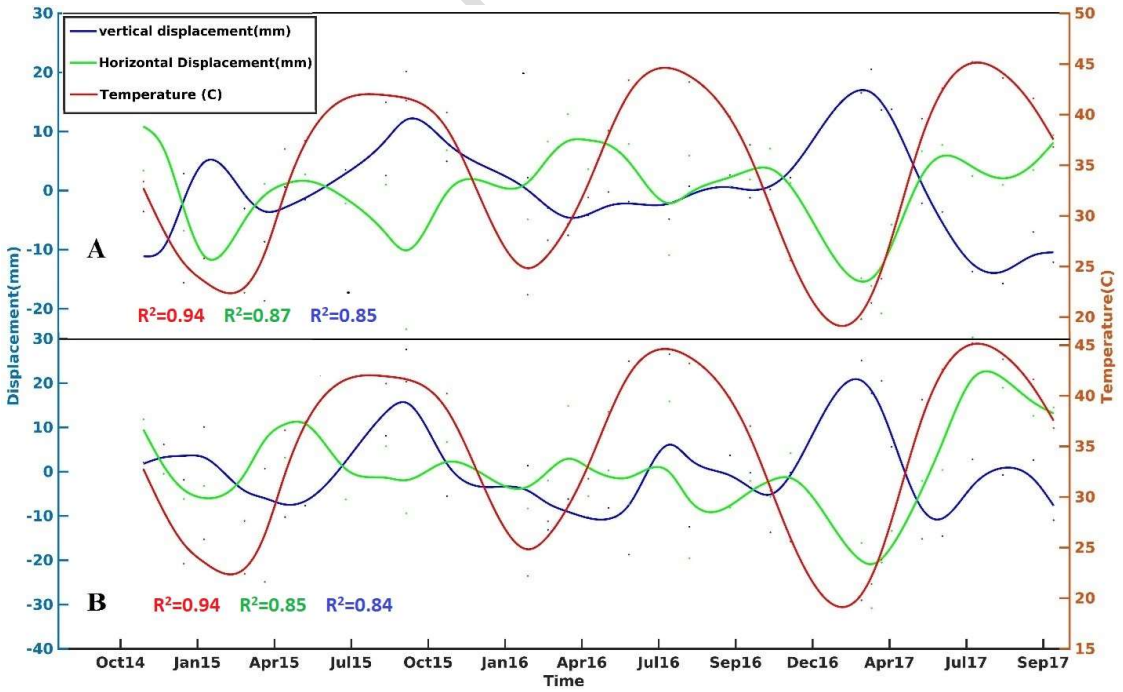

Figure 12. Vertical, Horizontal displacement and temperature time series of points 1(A) and 2(B) on the MZJ surface. The left and the right vertical axes show displacement and temperature respectively. Positive values of displacement correspond to uplift and westward movement while negative values correspond to subsidence and eastward movement

Conclusions

InSAR maps demonstrate that MZJ is one of the most active salt structures in the ZFTB, with a maximum uplift rate of ~15 mm/year and a maximum horizontal displacement of ~30 mm/year. The tectonic background and geomorphic properties combined with extracted horizontal and vertical movement suggest that the MZJ subaerial salt reached the surface after initial shortening across the ZFTB. The salt in MZJ then accumulated above the feeding vent, and formed a droplet, by increasing its thickness and weight. Then it spread gravitationally downslope and formed a Namakier which surrounds a central summit dome by the effect of the meteoric waters. The distribution of movement rate and direction shows that the central dome is spreading in three directions and forms a lobate pattern of horizontal movement. The central dome of The MZJ as foci of maximum movements shows the northeastern permanently uplifting zone, NW and SE subsiding zone, and the peripheral seasonal behavior which is regulated by wet and dry seasons. It can be concluded that the RS is one of the best methods for capturing the spatiotemporal evolution of natural high-activity structures such as subaerial MZJ salt diapir. However, the in situ measurements should be used to track the effects of dissolution and erosion as well as to assess the accuracy of extracted surface displacements.

Author's contributions

Arash jamshidy: Writing - original draft, Software, Methodology, Investigation, Data Curation,Conceptualization. Saeed madanipour: Writing - review & editing, Supervision, Formal analysis. Zahra Mousavi: Writing - review & editing, Methodology, Resources.

Conflicts of Interest

The authors declare no conflict of interest.

References

Abdolmaleki, N., Motagh, M., Bahroudi, A., Sharifi, M. A., Haghshenas Haghighi, M., 2014. Using Envisat InSAR time-series to investigate the surface kinematics of an active salt extrusion near Qum, Iran: Journal of Geodynamics, 81: 56-66.

Alavi, M., 1994. Tectonics of the Zagros Orogenic Belt of Iran: New Data Interpretation: Tectonophysics, 229: 211-238.

Bahroudi, A., Koyi, H. A., 2004. Tectono-sedimentary framework of the Gachsaran Formation in the Zagros forel basin: Marine Petroleum Geology, 21: 1295-1310.

Agard, P., Omrani, J., Jolivet, L., Mouthereau, F., 2005. Convergence history across Zagros (Iran): Constraints from collisional earlier deformation: International Journal of Earth Sciences, 94: 401-419.

Ajayebi, K.S., Amrikazemi, A., 2023. Geotourism in Iran. In: Allan, M.,Dowling, R. (Ed.), Geotourism in the Middle East: Geoheritage, Geoparks, Geotourism. Springer, 195-213.

Ala, M. A., 1974. Salt diapirism in southern Iran: American Association of Petroleum Geologists Bulletin, 58: 758-770.

Allen, K., 1972. Eminence Dome - natural gas storage in salt comes of age: Journal of Petroleum Technology, 24: 1299-1301.

Barber, D. E., Stockli, D. F., Horton, B. K., Koshnaw, R. I., 2018. Cenozoic exhumation and foreland basin evolution of the Zagros orogeny during the Arabia-Eurasia collision, western Iran: Tectonics, 37: 4396-4420.

Barnhart, W. D., Lohman, R. B., 2013. Phantom earthquakes and triggered aseismic creep: Vertical partitioning of strain during earthquake sequences in Iran: Geophysical Research Letters, 40: 819-823.

Barnhart, W.D.,Lohman, R.B., 2012. Regional trends in active diapirism revealed by mountain range-scale InSAR time series: Geophysical Research Letters, 39: L08309.
Barthel, R.,Haaf, E., Nygren, M., 2022. Systematic visual analysis of groundwater hydrographs: Potential benefits and challenges: Hydrogeology Journal, 30: 359-378.
Bekaert, D.P.S., Walters, R.J., Wright, T.J., Hooper, A.J., Parker, D.J., 2015. Statistical comparison of InSAR tropospheric correction techniques: Remote Sensing of Environment, 169: 321-331.
Berardino, P., Fornaro, G., Lanari, R.,Sansosti, E., 2002. A new algorithm for surface deformation monitoring based on small baseline differential SAR interferograms: IEEE Transactions on Geoscience Remote Sensing, 40: 2375-2383.
Berberian, F., Berberian, M., 1981. Tectono-plutonic episodes in Iran. In: Gupta, H. K., Delany, F. M. (Ed.), Zagros-Hindu Kush-Himalaya Geodynamic Evolution. AGU, 5-32.
Bruthans, J., Asadi, N., Filippi, M., Vilhelm, Z., Zare, M., 2007. A study of erosion rates on salt diapir surfaces in the Zagros Mountains, SE Iran: Environmental Geology, 53: 1079-1089.
Bürgmann, R., Rosen, P.A., Fielding, E.J., 2000, Synthetic aperture radar interferometry to measure Earth's surface topography and its deformation: Annual Review of Earth Planetary Sciences, 28: 169-209.
Chang, F., Dong, S., Yin, H., Wu, Z., Wang, W., 2023. Kinematic response of subaerial salt diapirs to geomorphic, tectonic and climatic regimes: Insights from space-based observations in the western Kuqa fold-thrust belt, NW China: Tectonics, 42:2022TC007670.
Chang, F., Dong, S., Yin, H., Wu, Z., Wang, W., 2022. Using the SBAS InSAR technique to monitor surface deformation in the Kuqa fold-thrust belt, Tarim Basin, NW China: Journal of Asian Earth Sciences, 231: 105212.
Colón, C., Webb, A. A., Lasserre, C., Doin, M.-P., Renard, F., Lohman, R., 2016. The variety of subaerial active salt deformations in the Kuqa fold-thrust belt (China) constrained by InSAR: Earth Planetary Science Letters, 450: 83-95.
Dalstrom, C. D. C., 1990. Geometric constraints derived from the law of conservation of volume applied to evolutionary models for detachment folding: American Association of Petroleum Geologists Bulletin, 75: 336-344.
Delgado Blasco, J.M., Foumelis, M., Stewart, C., Hooper, A., 2019. Measuring urban subsidence in the Rome metropolitan area (Italy) with Sentinel-1 SNAP-StaMPS persistent scatterer interferometry: Remote Sensing, 11: 129.
Dooley, T. P., Jackson, M. P., Hudec, M. R., 2009. Inflation and deflation of deeply buried salt stocks during lateral shortening: Journal of Structural Geology, 31: 582-600.
Edgell, H. S., 1996, Salt tectonism in the Persian Gulf Basin, In: Alsop, G. I., Blundell, D. J., Davison, I. (Ed.), Salt Tectonics. Geological Society Special Publications, 129-151.
Emami, H., 2008, Foreland propagation of folding and structure of the Mountain Front Flexure in the Pusht-e Kuh arc (NW Zagros, Iran) (PhD thesis): University of Barcelona, Barcelona.
Engl , P., McKenzie, D., 1982. A thin viscous sheet model for continental deformation: Geophysical Journal Royal Astronomical Society, 70: 295-321.
Farr, T.G., Kobrick, M., 2000, Shuttle Radar Topography Mission produces a wealth of data: EOS Transactions, 81: 583-585.
Ferretti, A., Prati, C., Rocca, F., 2001, Permanent scatterers in SAR interferometry: IEEE Transactions on Geoscience Remote Sensing, 39: 8-20.
Fuhrmann, T., Garthwaite, M. C., 2019, Resolving three-dimensional surface motion with InSAR: Constraints from multi-geometry data fusion: Remote Sensing, 11: 241.
Ghassemi, M., Roustaei, M., 2021, Salt extrusion kinematics: Insights from existing data, morphology and InSAR modeling of the active emergent Anguru diapir in the Zagros fold thrust belt, Iran: Journal of the Geological Society, 178: jgs2020-136.
Haaf, E., Barthel, R., 2018. An inter-comparison of similarity-based methods for organisation classification of groundwater hydrographs: Journal of Hydrology, 559: 222-237.
Hanssen, R. F., 2001. Radar Interferometry: Data Interpretation and Error Analysis Vol. 2: Springer Science & Business Media.
Harrison, J. V., 1930. The geology of some salt diapirs in Laristan: Quarterly Journal of the Geological Society of London, 86: 463-522.
Hassanpour, J., Yassaghi, A., Muñoz, J. A., & Jahani, S., 2021. Salt tectonics in a double salt-source

layer setting (Eastern Persian Gulf, Iran): Insights from interpretation of seismic profiles and sequential cross-section restoration: Basin Research, 33: 159-185.
Hessami, K., Koyi, H. A., Talbot, C. J., 2001. The significance of strike-slip faulting in the basement of the Zagros fold thrust belt: Journal of Petroleum Geology, 24(1): 5-28.
Hessami, K., Nilforoushan, F., Talbot, C. J., 2006. Active deformation within the Zagros Mountains deduced from GPS measurements: Journal of the Geological Society, 163: 143-148.
Homza, T., Wallace, W., 1995. Geometric kinematic models for detachment folds with fixed and variable detachment depths: Journal of Structural Geology, 17(4): 575-588.
Hooper, A., 2008, A multi-temporal InSAR method incorporating both persistent scatterer and small baseline approaches: Geophysical Research Letters, 35: L16302.
Hooper, A., Bekaert, D., Spaans, K., Arıkan, M., 2012, Recent advances in SAR interferometry time series analysis for measuring crustal deformation: Tectonophysics, 514-517: 1-13.
Hooper, A., Zebker, H., Segall, P., Kampes, B., 2004. A new method for measuring deformation on volcanoes and other natural terrains using InSAR persistent scatterers: Geophysical Research Letters, 31: 31, L23611.
Hudec, M. R., Jackson, M. P. A., 2007. Terra infirma: understing salt tectonics: Earth Science Reviews, 82: 1-28.
Huerford, A. J., Grunau, H. R., Stocklin, J., 1984. Fission track dating of an apatite crystal from Hormoz Island, Iran: Journal of Petroleum Geology, 7: 365-380.
Jahani, S., Callot, J.-P., Frizon de Lamotte, D., Letouzey, J., Leturmy, P., 2007. The salt diapirs of the eastern Fars province (Zagros, Iran): a brief outline of their past and present. In: Lacombe, O., Lave, J., Roure, F., Verges, J. (Ed.), Thrust Belts and Foreland Basins. Springer, Berlin, 289-308.
Jahani, S., Callot, J. P., Letouzey, J., Frizon de Lamotte, D., 2009. The eastern termination of the Zagros Fold-and -Thrust Belt, Iran: structures, evolution, and relationships between salt plugs, folding, and faulting: Tectonics, 28: TC6004.
Kent, P. E., 1958. Recent studies of south Persian salt diapirs: American Association of Petroleum Geologists Bulletin, 42: 2951-2972.
Khadivi, S., Mouthereau, F., Larrasoana, J. C., Verges, J., Lacombe, O., Khademi, E., Beamud, E., Melinte-Dobrinescu, M., Suc, J. P., 2010. Magnetochronology of synorogenic Miocene foreland sediments in the Fars arc of the Zagros Folded Belt (SW Iran): Basin Research, 22(6): 918-932.
Khorrami, F., Vernant, P., Masson, F., Nilfouroushan, F., Mousavi, Z., Nankali, H., Alijanzade, M., 2019. An up-to-date crustal deformation map of Iran using integrated campaign-mode and permanent GPS velocities: Geophysical Journal International, 217(2): 832-843.
Koshnaw, R. I., Stockli, D. F., Schlunegger, F., 2019. Timing of the Arabia-Eurasia continental collision—Evidence from detrital zircon U-Pb geochronology of the Red Bed Series strata of the northwest Zagros hinterl , Kurdistan region of Iraq: Geology, 47: 47-50.
Strohmenger, L., Sauquet, E., Bernard, C., Bonneau, J., Branger, F., Bresson, A., Brigode, P., Buzier, R., Delaigue, O., Devers, A., Evin, G., Fournier, M., Hsu, S.-C., Lanini, S., de Lavenne, A., Lemaitre-Basset, T., Mag , C., Mendoza Guimarães, G., Mentha, M., Munier, S., Perrin, C., Podechard, T., Rouchy, L., Sadki, M., Soutif-Bellenger, M., Tilmant, F., Tramblay, Y., Véron, A.-L., Vidal, J.-P., Thirel, G., 2023. On the visual detection of non-natural records in streamflow time series: challenges and impacts: Hydrology Earth System Sciences, 27: 3375-3391.
Li, J., Webb, A. A. G., Mao, X., Eckhoff, I., Colón, C., Zhang, K., 2014. Active surface salt structures of the western Kuqa fold-thrust belt, northwestern China: Geosphere, 10(6): 1219-1234.
Madanipour, S., Najafi, M., Nozaem, R., Vergés, J., Yassaghi, A., Heydari, I., Khodaparast, S., Soudm , Z., Aghajari, L., 2024. The Arabia-Eurasia collision zone in Iran: tectonostratigraphic and structural synthesis: Journal of Petroleum Geology, 47: 123-171.
Najafi, M., Beamud, E., Ruh, J., Mouthereau, F., Tahmasbi, A., Bernaola, G., Yassaghi, A., Motamedi, H., Sherkati, S., Goodarzi, M. G. H., Vergés, J., 2020. Pliocene growth of the Dowlatabad syncline in the Frontal Fars arc: Folding propagation across the Zagros Fold Belt, Iran: GSA Bulletin, 133(7-8): 1381-1403.
Massonnet, D., Rossi, M., Carmona, C., Adragna, F., Peltzer, G., Feigl, K., Rabaute, T., 1993. The displacement field of the Landers earthquake mapped by radar interferometry: Nature, 364: 138-142.
Mohammadnia, M., Najafi, M., Mousavi, Z., 2021. InSAR constraints on the active deformation of salt diapirs in the Kalut basin, Central Iran: Tectonophysics, 810: 228860.

Molinaro, M., Leturmy, P., Guezou, J.-C., Frizon de Lamotte, D., Eshraghi, S. A., 2005. The structure kinematics of the south-eastern Zagros fold-thrust belt, Iran: from thin-skinned to thick-skinned tectonics: Tectonics, 24: TC3007.

Motamedi, H., Sepehr, M., Sherkati, S., Pourkermani, M., 2011. Multi-phase Hormuz salt diapirism in the Southern Zagros, SW Iran: Journal of Petroleum Geology, 34(1): 29-44.

Motiei, H., 1995, Petroleum geology of Zagros: Geological Survey of Iran (in Farsi).

Mouthereau, F., Lacombe, O., Vergés, J., 2012. Building the Zagros collisional orogen: Timing, strain distribution and the dynamics of Arabia/Eurasia plate convergence: Tectonophysics, 532: 27-60.

Muchuru, S., Shepherd, J., Botai, J., Botai, C., L man, W., Adeola, A., 2015. Variability of rainfall over the Lake Kariba catchment area in the Zambezi River basin, Zimbabwe: Theoretical Applied Climatology, 124: 1-10.

Oveisi, B., Lave, J., van der Beek, P., Carcaillet, J., Benedetti, L., Aubourg, C., 2009. Thick-and thin-skinned deformation rates in the central Zagros simple folded zone (Iran) indicated by displacement of geomorphic surfaces: Geophysical Journal International, 176: 627-654.

Perotti, C., Chiariotti, L., Bresciani, I., Cattaneo, L., Toscani, G., 2016. Evolution timing of salt diapirism in the Iranian sector of the Persian Gulf: Tectonophysics, 679: 180-198.

Pirouz, M., Avouac, J.-P., Hassanzadeh, J., Kirschvink, J. L., Bahroudi, A., 2017. Early Neogene foreland of the Zagros, implications for the initial closure of the Neo-Tethys kinematics of crustal shortening: Earth Planetary Science Letters, 477: 168-182.

Pirouz, M., Simpson, G., Chiaradia, M., 2015. Constraint on foreland basin migration in the Zagros Mountain belt using Sr isotope stratigraphy: Basin Research, 27: 714-728.

Player, R. A., 1969. Salt Plug Study: Iranian Oil Operating Companies, Geological Exploration Division, Report No. 1146, (unpublished).

Scheiber, R., Moreira, A., 1999. Improving co-registration accuracy of interferometric SAR images using spectral diversity: IEEE 1999 International Geoscience Remote Sensing Symposium. IGARSS'99 (Cat. No.99CH36293), Hamburg, Germany, 1709-1711.

Ruh, J.B., Hirt, A.M., Burg, J.-P., Mohammadi, A., 2014. Forward propagation of the Zagros Simply Folded Belt constrained from magnetostratigraphy of growth strata: Tectonics, 33:1534-1551.

Samieie-Esfahany, S., Hanssen, R., van Thienen-Visser, K., Muntendam-Bos, A., 2009. On the effect of horizontal deformation on InSAR subsidence estimates: Proceedings of the Fringe 2009 Workshop, Frascati, Italy.

Samsonov, S., d'Oreye, N., 2012. Multidimensional time-series analysis of ground deformation from multiple InSAR data sets applied to Virunga Volcanic Province: Geophysical Journal International, 191(3): 1095-1108.

Samsonov, S., Dille, A., Dewitte, O., Kervyn, F., d'Oreye, N., 2020. Satellite interferometry for mapping surface deformation time series in one, two and three dimensions: A new method illustrated on a slow-moving land slide: Engineering Geology, 266: 1054-71.

Shami, S., Shahriari, M.A., Nilfouroushan, F., Forghani, N., Salimi, M., Reshadi, A., 2024. Surface displacement measurement and modeling of the Shah-Gheyb salt dome in southern Iran using InSAR machine learning techniques: International Journal of Applied Earth Observation and Geoinformation, 132, 10.1016/j.jag.2024.104016.

Sherkati, S., Molinaro, M., de Lamotte, D.F., Letouzey, J., 2005. Detachment folding in the Central Eastern Zagros fold-belt (Iran): Salt mobility, multiple detachments and late basement control: Journal of Structural Geology, 27(9): 1680-1696.

Sherkati, S., Letouzey, J., 2004. Variation of structural style and basin evolution in the central Zagros (Izeh zone and Dezful Embayment), Iran: Marine and Petroleum Geology, 21: 535-554.

Słotwiński, M., Krýza, O., Warsitzka, M., Závada, P., Adineh, S., 2023. Influence of cap-rock on deformation during extrusion of salt diapir - a numerical study: EGUsphere, 10.5194/egusphere-egu23-12189.

Snidero, M., Carrera, N., Mencos, J., Butillé, M., Granado, P., Tavani, S., Lopez-Mir, B., Sàbat, F., Muñoz, J.A., 2020. Diapir kinematics in a multi-layer salt system from the eastern Persian Gulf: Marine and Petroleum Geology, 117: 104402.

Song, P., Ding, L., Zhang, L., Cai, F., Zhang, Q., Li, Z., et al., 2023. Paleomagnetism from Central Iran reveals Arabia-Eurasia collision onset at the Eocene/Oligocene boundary: Geophysical Research Letters, 50: e2023GL103858.

Spiers, C.J., Urai, J.L., Lister, G.S., Bol , J.N., Zwart, H.J., 1986. The Influence of Fluid-Rock Interaction on the Rheology of Salt Rock: Final Report EUR 10399 EN, Utrecht, Netherlands: State University of Utrecht.

Talbot, C.J., Pohjola, V., 2009. Subaerial salt extrusions in Iran as analogues of ice sheets, streams glaciers: Earth-Science Reviews, 97: 167-195.

Talbot, C.J., Medvedev, S., Alavi, M., Shahrivar, H., Heidari, E., 2000. Salt extrusion rates at Kuh-e-Jahani, Iran: June 1994 to November 1997: Geological Society London Special Publications, 174, 93-110.

Talbot, C.J., Rogers, E., 1980. Seasonal movements in an Iranian salt glacier: Science, 208: 395-397.

Urai, J.L., Spiers, C.J., Zwart, H.J., Lister, G.S., 1986. Weakening of rock salt by water during long-term creep: Nature, 324(6097): 554-557.

Vernant, P., Nilfouroushan, F., Hatzfeld, D., Abbassi, M., Vigny, C., Masson, F., 2004. Contemporary crustal deformation and plate kinematics in Middle East constrained by GPS measurements in Iran northern Iran: Geophysical Journal International, 157: 381-398.

Zarei, M., Raeisi, E., Talbot, C.J., 2012. Karst development on a mobile substrate: Konarsiah salt extrusion, Iran: Geological Magazine, 149: 412-422.

Zhang, S., Jiang, Q., Shi, C., Xu, X., Gong, Y., Xi, J., Liu, W., Liu, B., 2021. Application of Sentinel-1 -2 Images in Measuring the Deformation of Kuh-e-Namak (Dashti) Namakier, Iran: Remote Sensing, 13(4): 785.